A Demonstration of Broadband RF Sensing: Empirical Polysilicon Etch Rate Estimation in a Lam 9400 Etch Tool

Craig Garvin and J. W. Grizzle

Department of Electrical Engineering and Computer Science,

University of Michigan

1301 Beal Ave, Ann Arbor, MI 48109-2122

{*garv, grizzle* }*@eecs.umich.edu*

Abstract

The sensitivity of a novel broad frequency band ($1 GHz$ to $2.25 GHz$) RF sensing system to plasma etching process conditions is demonstrated. This is accomplished by using the sensing system to estimate polysilicon etch rate in a Lam 9400 etch tool. A designed experiment varying physical and chemical reactive ion etching regimes was performed with five repetitions at each experimental point. A model relating broadband sensor response to etch rate was regressed using four repetitions of the data and validated on the fifth. Two representations of the broadband data were considered separately when regressing the models, with subset selection used in each case to choose the best predictor variables. In one representation, the sensor data was considered as a vector of 402 real numbers corresponding to magnitude and phase of reflection coefficient at each of 201 frequencies, resulting in an R^2 of etch rate estimate of 0.997. In the other, the broadband response was parameterized on the basis of a multi modal cavity resonance model. The inferred parameters of natural frequency, quality factor and resistance were then used as the predictor variables for regression, resulting in an R^2 of 0.962.

I. INTRODUCTION

A significant trend in microelectronics manufacturing is the movement towards closed loop control and real-time sensing and diagnostics in order to improve overall equipment efficiency, commonly referred to as 'advanced process control' (APC). This paper presents advances in real-time RF sensing and diagnostics for reactive ion etching (RIE), a critical microelectronics process step. RIE employs a plasma of reactive chemicals in a vacuum chamber to achieve precise and rapid material removal. RF sensing refers to the measurement of electrical properties of the plasma at radio frequencies (the megahertz to low gigahertz range) for the purpose of diagnostics and control of the process.

This article presents continued advances in the use of a novel RF sensing system for microelectronics process diagnostics, referred to as 'broadband' RF sensing. In Ref. [1], we introduced the broadband concept and demonstrated significantly better sensitivity to plasma parameters than standard RF sensing in a research reactor using simple chemistries. In this article, we present a minimally intrusive implementation of the broadband sensor on a Lam 9400, along with a demonstration of sensitivity to a process parameter, rather than plasma parameters. Sensitivity to a process parameter is demonstrated by obtaining an empirical etch rate estimation based solely on the broadband sensor response.

There is a long history of investigation of the electrical properties of processing plasmas by both passive and active means. We use 'passive sensing' to refer to methods that rely on the existing power supply to excite the plasma and add sensors to passively measure electrical characteristics at the drive frequency and any of its harmonics [2–9]. 'Active sensing' refers to approaches involving a separate frequency source and antenna to drive the plasma. In active sensing, a low power high frequency source typically drives the plasma over a range of frequencies rather than at single frequency. Nevertheless, standard active sensing approaches [10–19] have to date only used a single parameter from the frequency sweep: the frequency of minimum reflection or maximum transmission as the measured quantity. This 'resonance' frequency has been converted to plasma density [11–13].

Active sensing of contained plasmas has been described as early as 1952 by Brown and Rose [10]. The method was briefly considered for processing applications [16–19] in the mid 1980's, but the work of de Vries *et. al* [17] appears to have terminated this line of inquiry. Their work found poor correlation between the electron density estimated from active sensing and etch rate, suggesting the diagnostic had limited value. Our work is in complete agreement with de Vries, but we draw different conclusions. We confirm that when active sensing is used as a single parameter diagnostic, it does indeed correlate poorly with etch rate. However, we use this conclusion to motivate the use of the full frequency response spectrum provided by the RF sensor. By employing multi parameter empirical analysis, similar to Refs. [20–22], we are able to estimate etch rate to a high degree of accuracy. We are also able to achieve accurate etch rate estimation with a multi-parameter model of the broadband response that considers changes in resonant frequency and quality factor not just at the primary resonant mode of the cavity, but at several excited modes.

II. EXPERIMENTAL SETUP

The experimental work involves etching of blanket polysilicon wafers in a LAM 9400 reactor equipped with broadband RF sensing. A more detailed discussion of each element follows.

As depicted in Figure 1, the spacer plate of our Lam 9400 has been modified with optical ports. For convenience, we convert one of the unused optical ports to a broadband probe. The optical port has a 9.5 mm diameter aperture with 0° elevation angle, radially aligned with the center of the chamber. The probe design is shown in Figure 2. A quartz tube sealed by O-rings serves to insulate the antenna from the discharge. Inside the quartz tube, a length of MIL-17C tin plated aluminum, semi-rigid coaxial cable acts as a monopole antenna. In its present form, a 13 mm antenna is used, located 75 mm from the outer wall of the chamber and about 100 mm above the substrate.

A Hewlett Packard 8753B network analyzer drives the broadband probe over a range of $1\,GHz$ to $2.25 GHz$ at a power level of 0 dBM. After calibration, the complex reflection coefficient ($\mathbf{\Gamma}$)

is recorded at 201 frequency points linearly uniformly spaced between $1\,GHz$ and $2.25\,GHz$. The set-points of power, pressure and flow rate for the LAM 9400 as well as data acquisition are controlled with PC's running LabVIEW data acquisition and control software and linked via Data Socket [23]. The broadband data are acquired at a sample rate of 5 Hz while all other data are acquired at 10 Hz. Broadband data over the duration of an experiment are averaged on a frequency-by-frequency basis for the purpose of regressing etch rate. All data are logged and written to file automatically.

The substrate etched in all experiments is a 6 inch silicon wafer composed of 5000 Å unpatterned undoped polysilicon, over 300 Å thermal oxide, over crystalline silicon. For the purposes of this experiment, the oxide layer serves as a reflective boundary to enable the determination of the polysilicon thickness. Thickness was measured before and after each etch using a Leitz SP, and rate was calculated from thickness and total etch time.

III. EXPERIMENT DESIGN AND INITIAL DISCUSSION

Reactive ion etching consists of two dominant etch mechanisms - physical and chemical. Our goal in this experiment will be to keep electron density roughly constant while varying the relative importance of the physical and chemical etch components. Based on the results of Ra [24] in a chamber similar to ours, we keep electron density constant by maintaining a constant TCP power. High and low ion energy is achieved through the choice of bias power. The chemical component of the etch is varied from 'passivating' to 'etching' by varying the relative flow of HBr and Cl_2. In each case, total flow rate is kept constant in order to maintain a roughly constant overall residence time. The chosen levels of the experimental variables are shown in Table I. Five repetitions of the experiment were performed in fully random order, for a total of 20 experiments.

Figure 3 shows a typical response of the broadband sensor for each of the four treatment combinations. For each case, we see that the response is composed of two resonant peaks. We will refer to the lower frequency peak as the primary mode, M_1, and the higher frequency peak as the secondary mode, M_2. In keeping with previous work in this area [10–19], we will assume that

these peaks are due to resonant modes in an enclosure filled with a lossy dielectric. If we assume the standard perturbation model [25], then each mode is represented as a series RLC circuit. With this model, it is clear that two modes are insufficient to describe the response of Figure 3. We see that the primary mode, M_1, clearly has additional structure beyond the main resonance peak, and to a lesser extent so does M_2. Accordingly, we propose two additional degenerate modes: $M_1^{'}$, and $M_2^{'}$ to account for the additional features in each resonance. Consequently, each mode can be described by its resonant frequency, ω_n, quality factor, Q, and minimum reflection coefficient magnitude, $|\mathbf{\Gamma}_{min}|$ or resistance[1], R. To illustrate the notation, $(\omega_n)_1^{'}$ denotes the resonant frequency of the degenerate primary mode, while $|\mathbf{\Gamma}_{min}|_2$ denotes the minimum reflection coefficient of the secondary mode.

Having established the notation, let us now observe that the resonant frequency of the primary mode, $(\omega_n)_1$, does not correlate with changes in etch rate. Etch rate increases both with the change from passivating to etch chemistry, and with the change from low to high bias power. $(\omega_n)_1$ increases with the switch from passivating to etch chemistry, but *decreases* with increasing bias power. This poor correlation is not surprising, since the experimental goal was to vary etch rate while keeping electron density, and thus $(\omega_n)_1$, roughly constant. The lack of correlation between $(\omega_n)_1$ and etch rate confirms the observation of de Vries *et. al* and motivates considering more subtle features of the broadband data.

We note that the prominence of the degenerate primary mode, $M_1^{'}$, changes significantly with process conditions. $(|\mathbf{\Gamma}_{min}|)_1$, $(|\mathbf{\Gamma}_{min}|)_2$ and Q_2 change as well. All of these can serve as potential indicators. The question of whether these changes are sufficiently reliable to accurately predict etch rate is addressed in Section V, with a regression model .

---

[1]Using an RLC circuit model, R is equivalent to $|\mathbf{\Gamma}_{min}|$, since $\mathbf{\Gamma}_{min} = \frac{\mathbf{R}-\mathbf{Z_o}}{\mathbf{R}+\mathbf{Z_o}}$. From a plot of $|\mathbf{\Gamma}|$ vs ω, $|\mathbf{\Gamma}_{min}|$ is directly observed while R is not. Conversely, a transfer function representation is more readily formulated with R

IV. BROADBAND PARAMETERIZATION BY MULTI MODAL CAVITY RESONANCE PERTURBATION MODEL

A single sweep of the broadband RF measurement results in 402 real numbers: the log-magnitude of the reflection coefficient, $\log(|\mathbf{\Gamma}|)$, and its phase, $\arg(\mathbf{\Gamma})$, at 201 linearly uniformly spaced frequency points from $1\,GHz$ to $2.25\,GHz$. Consequently, the measurement set results in a vastly over-determined regression problem from RF data to etch rate. We address this over-abundance of data in two ways. In the 'purely empirical' approach, we use a subset selection methodology [26–28], described in Appendix A, directly on the 402 element vector of RF data. The result of the subset selection procedure is that magnitudes and phases at specific frequencies are used for the etch estimate, and all other values of magnitude and phase are ignored. An alternative is the 'parametric' approach. Here, the broad band frequency sweep is represented by the circuit parameters of four RLC circuits, thus reducing 402 points to 12. The same subset selection methodology is used on these circuit parameters to build a regression model relating *circuit parameters* to etch rate. The circuit parameters are derived as follows:

It is well established [25] that a cavity filled with a lossless homogeneous dielectric can be approximated by a series LC circuit for each propagating mode, with the LC circuits in parallel to each other, as shown in Figure 4. For lossy inhomogeneous dielectrics, a perturbation analysis [11–13, 29] leads to an RLC circuit. In this model, the natural frequency, ω_n, and quality factor, Q, of each mode is perturbed by the presence of plasma. A finite Q can be modeled by the addition a resistance to each LC circuit in Figure 4. As we have noted in Section III, four modes, resulting in four RLC circuits, appear sufficient to capture the broadband response. Using this model structure, the complex reflection coefficient as a function of frequency, $\mathbf{\Gamma}(\omega)$, is simply the admittance of four series RLC circuits in parallel converted to a reflection coefficient, as we will illustrate:

We begin by calculating the admittance of a series RLC circuit:

$$Y(s) = \frac{\frac{2\omega_n}{RQ}s}{s^2 + \frac{2\omega_n}{Q}s + \omega_n^2} \tag{4.1}$$

Because standard equations [11–13, 29] relate plasma density and collision frequency to natural frequency and quality factor, we express admittance in terms of ω_n and Q rather than L and C.

Since parallel admitances add, the total admittance, Y_{tot}, resulting from four RLC circuits in parallel is:

$$Y_{\rm tot} = \sum_{k=1}^{4} \frac{\frac{2(\omega_n)_k}{R_k Q_k} s}{s^2 + \frac{2(\omega_n)_k}{Q_k} s + \omega_{n_k}^2} \tag{4.2}$$

Since we measure reflection coefficient, and not admittance, we express reflection coefficient in terms of admittance:

$$\mathbf{\Gamma}(\omega) = \frac{\mathbf{1} - \mathbf{Z}_\circ \mathbf{Y}_{\rm tot}}{\mathbf{1} + \mathbf{Z}_\circ \mathbf{Y}_{\rm tot}} \tag{4.3}$$

Once we have an expression for $\mathbf{\Gamma}(\omega)$ from Eq. 4.3, we use a standard nonlinear optimization routine to minimize the difference between the modeled and measured reflection coefficient and obtain the parameters ω_n, Q and R for each mode. In addition to these three, the mode parameters were augmented with certain nonlinear transformations described as follows: The quality factor Q of a given mode corresponds to the amount of damping. Damping is often represented by a 'damping coefficient', $\sigma = \frac{1}{Q}$, and both Q and σ are included. In a similar vein, R, $|\mathbf{\Gamma}_{min}|$ and $\text{VSWR}(\mathbf{\Gamma}_{min})$ [2] are all included. The final set of 'parameter' broadband data, $\mathbf{M}_p$ is:

$$\begin{aligned} \mathbf{M}_p = \big[&(\omega_n,\, Q,\, R,\, \sigma,\, |\mathbf{\Gamma}_{min}|\,,\, \text{VSWR}(\mathbf{\Gamma}_{min}))_{\mathbf{1}} \ldots \\ &\ldots (\omega_n,\, Q,\, R,\, \sigma,\, |\mathbf{\Gamma}_{min}|\,,\, \text{VSWR}(\mathbf{\Gamma}_{min}))_{\mathbf{2}}^{'}\big]\,,\ \mathrm{M_p} \in \Re^{20\times 24} \end{aligned} \tag{4.4}$$

V. EXPERIMENTAL RESULTS

We first consider the performance of the 'purely empirical' model based on the 402 points of raw RF measurement. The subset selection methodology of Appendix A was used to regress a model based on 4 repetitions of the data which was then evaluated on the fifth data set. This was repeated in a round-robin fashion and the 'goodness of fit' R^2 was determined based on all 5 permutations. The result is an extremely good fit of $R^2 = 0.997$, corresponding to an *RMS* error

[2] $\text{VSWR}(\mathbf{\Gamma}) = \frac{\mathbf{1}+|\mathbf{\Gamma}|}{\mathbf{1}-|\mathbf{\Gamma}|}$

of 0.8%. Figure 5 shows the actual etch rate obtained from Leitz SP thickness measurement and etching time, as well as the etch rate prediction based on the broadband signal. Figure 6 illustrates typical magnitude and phase points selected to regress the etch rate model. We note that all the selected points are in areas of relatively low absorption ($|\log(|\mathbf{\Gamma}_{min}|)| < 10$dB), which is somewhat surprising.

We also regress a model based on the parameters of four resonant modes, shown in Eq. (4.4). The fit achieved with the parameterized approach is almost as good as the purely empirical fit: $R^2 = 0.962$. Table II lists the mode parameters in the order than they contribute to fitting etch rate. The most significant contribution is that of $(\omega_n)_1^{'}$, the resonant frequency of the *degenerate* primary mode. Furthermore, $(\omega_n)_1$, the resonant frequency of the primary mode is very *insignificant*, and shows up well beyond the cutoff for reasonable model order. However, the other two features of M_1, R_1 and Q_1, are both significant. $R_1^{'}$ is significant, but as a standing wave ratio ($\text{VSWR}_1^{'}$). Finally, whereas $(\omega_n)_1$ was not significant, the only significant component of M_2 is $(\omega_n)_2$.

VI. CONCLUSION

A novel RF sensing system based on multi-mode microwave excitation of a plasma chamber was implemented on a LAM 9400 etch tool. A four level experiment was designed with the goal of relating polysilicon etch rate to RF measurement. Using only information from the broadband RF sensor, etch rate was estimated with an an average R^2 of 0.997, using a purely empirical model, and an R^2 of 0.962 with a model based on an equivalent circuit representation of the broadband response.

The next step towards process control with broadband RF sensing is to move from accurate prediction of discrete points to a model that can interpolate over a reasonable operating range. Once such a model is developed, it will be possible to incorporate the broadband RF response into an advanced process control strategy. Additionally, more relevant process conditions such as etching of patterned wafers must be considered.

ACKNOWLEDGMENTS

Mr. Pete Klimecky assisted with sample preparation and experimental work. Dr. Sven Bilen built the broadband antenna.

This work was supported in part by AFOSR/ARPA MURI Center under grant # F49620-95-1-0524 and The Semiconductor Research Company under contract #97-FC-085. C. Garvin is supported by an Intel Foundation Fellowship.

APPENDIX A: SUBSET SELECTION

This appendix presents the model regression technique used in this paper. A discussion of subset selection can be found in [26–28].

In both the 'purely empirical' and 'parametric' modeling approaches, we begin with a set of measured variables, $\mathbf{M}_e$ (empirical) or $\mathbf{M}_p$ (parametric):

$$\mathbf{M}_e = [\log|\mathbf{\Gamma}(\omega)|),\ \arg(\mathbf{\Gamma}(\omega))]\,, \tag{A1}$$

$$\mathbf{\Gamma}(\omega) \in \mathbb{C}^{\mathbf{20\times 201}},\ \mathrm{M_e} \in \Re^{20\times 402}$$

$$\mathbf{M}_p = [(\omega_n,\ Q,\ R,\ \sigma,\ |\mathbf{\Gamma}_{min}|\,,\ \mathrm{VSWR})_1 \ldots$$

$$(\omega_n,\ Q,\ R,\ \sigma,\ |\mathbf{\Gamma}_{min}|\,,\ \mathrm{VSWR})_2'\big]\,,\ \mathrm{M_p} \in \Re^{20\times 24} \tag{A2}$$

In all cases, the response variable is a vector of 20 values of etch rate, $\mathbf{ER}$. We will partition the matrix M along both rows and columns and the vector $\mathbf{ER}$ by rows.

We partition $\mathbf{M}_e$, $\mathbf{M}_p$ and $\mathbf{ER}$ by rows to form a modeling set and test set:

$$\mathbf{M}_e = \left[\frac{M_e}{\mathcal{M}_e}\right],\ \text{model: } M_e \in \Re^{16\times 402},\ \text{test: } \mathcal{M}_e \in \Re^{4\times 402}, \tag{A3}$$

$$\mathbf{ER} = \left[\frac{Y}{\mathcal{Y}}\right],\ \text{model: } Y \in \Re^{16\times 1},\ \text{test: } \mathcal{Y} \in \Re^{4\times 1}. \tag{A4}$$

The partition is the same for $\mathbf{M}_p$. For all symbols, Roman font is the entire data, italics, the modeling set and calligraphic the test set. All 5 permutations of a modeling set composed of 4

repetitions of the experimental conditions and a test set composed of the remaining repetition are used to evaluate etch estimation. Unless specifically stated otherwise, data guiding model design is exclusively obtained from $[X, Y]$ and data on model performance is exclusively obtained from $[\mathcal{X}, \mathcal{Y}]$.

We partition $\mathbf{M}$ by columns to form the matrix of predictor variables, $\mathbf{X}$. A specific column of $\mathbf{M}$, $\mathbf{m}_i$, represents a particular measurement variable. We can use any subset of $\mathbf{M}$, specified by a set of indices, α, to form the matrix of predictor variables:

$$\mathbf{X} = [\mathrm{m}_{\alpha_1} \ldots \mathrm{m}_{\alpha_n}] \tag{A5}$$

$$\alpha = \text{set of indices} \tag{A6}$$

$$n = \text{model order} \tag{A7}$$

$$\mathbf{X} = \left[\frac{X}{\mathcal{X}}\right], \text{ model: } X \in \Re^{16\times n}, \text{ test: } \mathcal{X} \in \Re^{4\times n}, \tag{A8}$$

Given α, we partition $\mathbf{X}$ into X and $\mathcal{X}$ and regress a model, B on the modeling set:

$$B = (X^{'} \cdot X)^{-1} \cdot X^{'} \cdot Y \tag{A9}$$

We use B to estimate etch rate on the test set:

$$\widehat{\mathcal{Y}} = \mathcal{X} \cdot B, \tag{A10}$$

and quantify estimate performance with:

$$R^2 = 1 - \frac{\sum_{k=1}^{n}(\widehat{y}_i - y_i)^2}{\sum_{k=1}^{n}(y_i - \bar{\mathcal{Y}})^2}, \tag{A11}$$

Determining the optimal α is a computationally explosive problem [26]. An effective approximation of an optimal α can be achieved by forward selection followed by backwards elimination [26].

Forward selection is accomplished by the following iterative algorithm:

$$X_i^{\mathrm{temp}} = [X_j^{\mathrm{best}} \vdots x_i], \tag{A12}$$

$$\widehat{Y_i} = X_i^{\mathrm{temp}} \cdot [(X_i^{\mathrm{temp}})^{'} \cdot X_i^{\mathrm{temp}}]^{-1} \cdot (X_i^{\mathrm{temp}})^{'} \cdot Y \tag{A13}$$

$$E_i = \|Y - \hat{Y}_i\|_2, \tag{A14}$$

$$i^\star = \mathrm{ARG}[\min(\mathrm{E_i})], \tag{A15}$$

$$X_{j+1}^{\mathrm{best}} = X_{i^\star}^{\mathrm{temp}}. \tag{A16}$$

We begin with X_1^{best} equal to a mean term. We then form X_i^{temp}, a candidate for the next largest X^{best}, using each variable in X in sequence. We then calculate the error E_i obtained using each candidate X_i^{temp} and determining $\hat{Y}_i$ using Eq. A13. We select the best candidate $X_{i^\star}^{\mathrm{temp}}$ to be the next largest X^{best}. The algorithm is terminated when X^{best} contains 16 elements.

Once the subset of variables X^{best} has been selected, we re-order it by reversing Equations A12-A16, resulting in backwards elimination:

$$X_i^{\mathrm{temp}} = [x_1 \cdots x_{i-1}\ x_{i+1} \cdots x_j] \mid x \in X_j^{\mathrm{best}}, \tag{A17}$$

$$\widehat{Y_i} = X_i^{\mathrm{temp}} \cdot [(X_i^{\mathrm{temp}})' \cdot X_i^{\mathrm{temp}}]^{-1} \cdot (X_i^{\mathrm{temp}})' \cdot Y \tag{A18}$$

$$E_i = \|Y - \hat{Y}_i\|_2, \tag{A19}$$

$$i^\star = \mathrm{ARG}[\min(\mathrm{E_i}), \tag{A20}$$

$$X_{j-1}^{\mathrm{ord}} = X_{i^\star}^{\mathrm{temp}}. \tag{A21}$$

We begin with $X_j^{\mathrm{ord}} = X_j^{\mathrm{best}}$, $j = 16$. We form j X_i^{temp}'s, each missing the i^{th} variable. The variable $x_{i^\star}$ is the component of X_j^{best} that *least* contributes to fitting Y. Accordingly, X_{j-1}^{ord} is formed from X_j^{ord} by eliminating $x_{i^\star}$. Once the process is repeated to $j = 1$ the result is a set of variables ordered by their ability to predict Y.

An 'F-test' is used to determine model order as follows: Given two models of size n and m, $n > m$, and the mean squared error, E_n and E_m, achieved using models of size n and m the F-test gives the likelihood that the reduction in error is due to chance. We can apply the F-test to models based on $X_i^{\mathrm{ord}}\ |_{i=1}^{16}$. Once the probability that the improvement from X_{i+1}^{ord} to X_i^{ord} is due to chance is greater than 5%, we determine that the best model size, $n^\star$, has been reached. For the 'empirical' approach, $n^\star = 7$, for the 'parametric' approach, $n^\star = 5$.

We then use the model, B, built with $X_{1:n^\star}^{\mathrm{ord}}$ and evaluate it on test set. The process is then repeated for the four remaining permutations of model and test set in round robin fashion.

REFERENCES

[1] C. Garvin, D. S. Grimard, and J. W. Grizzle, J. Vac. Sci. Technol. A **17**, 1377 (1999).

[2] M. A. Sobolewski, IEEE Transactions on Plasma Sciences **23**, 1006 (1995).

[3] M. A. Sobolewski, J. K. Olthoff, and Y. C. Wang, J. Appl. Phys. **85**, 3966 (1999).

[4] J. H. Keller and W. B. Pennebaker, IBM J. Res. Develop. **23**, 3 (1979).

[5] V. A. Godyak, R. B. Piejak, and B. M. Alexandrovich, J. Appl. Phys. **69**, 3455 (1991).

[6] J. W. Butterbaugh, L. D. Baston, and H. H. Sawin, J. Vac. Sci. Technol. A **8**, 916 (1990).

[7] M. Klick, J. Appl. Phys. **79**, 3445 (1996).

[8] S. Wurm, W. Preis, and M. Klick, Solid State Tech. **42**, 103 (1999).

[9] S. Reeves and C. Fullwood, in *IEEE/SEMI Advanced Semiconductor Manufacturing Conference and Workshop* (IEEE, Piscataway, NJ, 1994), pp. 298–304.

[10] D. J. Rose and S. Brown, J. Appl. Phys. **23**, 1028 (1952).

[11] M. A. Heald and C. B. Wharton, *Plasma diagnostics with microwaves* (John Wiley and Sons, New York, NY, 1965).

[12] P. E. Vandenplas, *Electron Waves and Resonances in Bounded Plasmas* (John Wiley and Sons, London, 1968).

[13] A. Gilardini, *Low Energy Electron Collisions in Gases* (John Wiley and Sons, New York, NY, 1972).

[14] C. B. Wharton, R. F. Post, and T. Prosser, Lawrence Radiation Lab Report **5**, 238 (1955).

[15] R. S. Harp and F. W. Crawford, J. Appl. Phys. **35**, 3436 (1964).

[16] C. B. Fleddermann, J. H. Beberman, and J. T. Verdeyen, J. Appl. Phys. **58**, 1344 (1985).

[17] C. A. M. de Vries, A. J. van Roosmalen, and G. C. C. Puylaert, J. Appl. Phys. **57**, 4386

(1985).

[18] R. M. Moroney, A. J. Lichtenberg, and M. A. Lieberman, J. Appl. Phys. **66**, 1618 (1989).

[19] M. Haverlag, G. M. W. Kroesen, T. H. J. Bisschops, and F. J. Dehoog, Plasma chemistry and plasma processing **11**, 357 (1991).

[20] R. Shadmehr *et al.*, J. Echem. Soc. **139**, 907 (1992).

[21] R. Chen, H. Huang, C. J. Spanos, and M. Gatto, J. Vac. Sci. Technol. A **14**, 901 (1996).

[22] D. White, D. Boning, and G. Butler, S. W. Barna, IEEE Transactions on Semiconductor Manufacturing **10**, 52 (1997).

[23] P. Klimecky, D. Schweiger, and J. W. Grizzle, in *Abstracts of the* 195^{th} *Electrochemical Society Meeting* (Electrochemical Society, Pennington, New Jersey, 1999), Vol. 195, p. 214.

[24] Y. Ra, S. G. Bradley, and C. H. Chen, J. Vac. Sci. Technol. A **12**, 1328 (1994).

[25] J. C. Slater, Rev. Mod. Phys. **18**, 441 (1946).

[26] A. J. Miller, *Subset Selection in Regression* (Chapman and Hall, New York, New York, 1990).

[27] A. Sen and M. Srivastava, *Regression Analysis: Theory, Methods, and Applications* (Springer-Verlag, New York, New York, 1990).

[28] J. Neter, W. Wasserman, and M. H. Kutner, *Applied Linear Statistical Models* (Richard D. Irwin, Inc, New York, New York, 1985).

[29] M. A. Biondi and S. Brown, Phys. Rev. **75**, 1700 (1949).

FIGURES

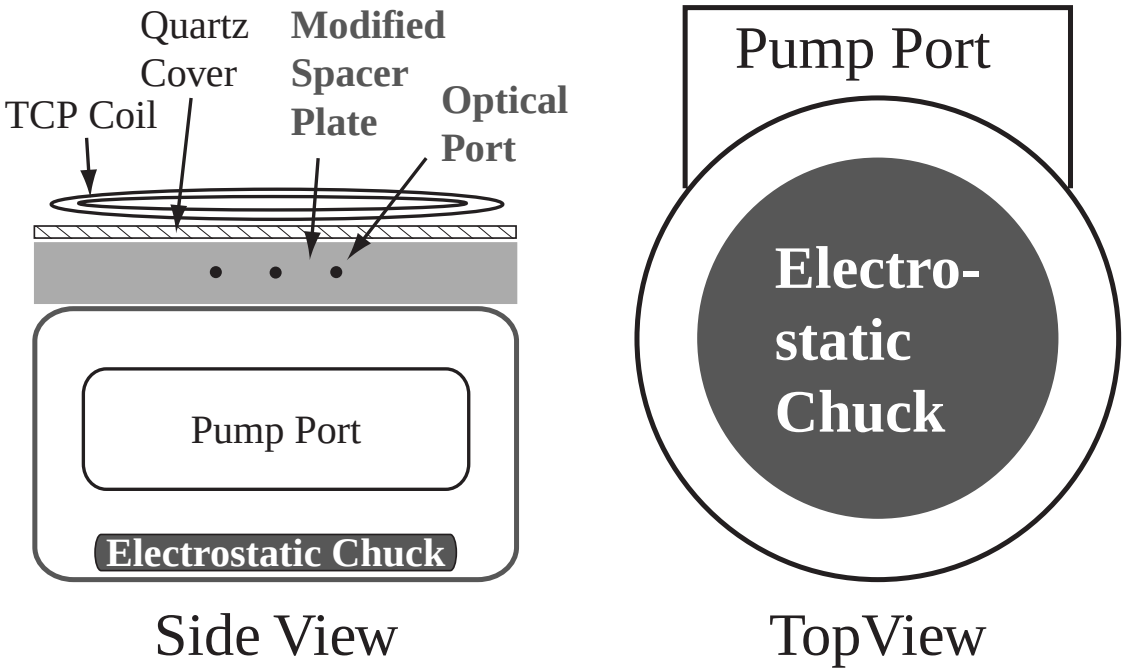

FIG. 1. Schematic of Lam 9400, showing modification of spacer plate to include optical ports

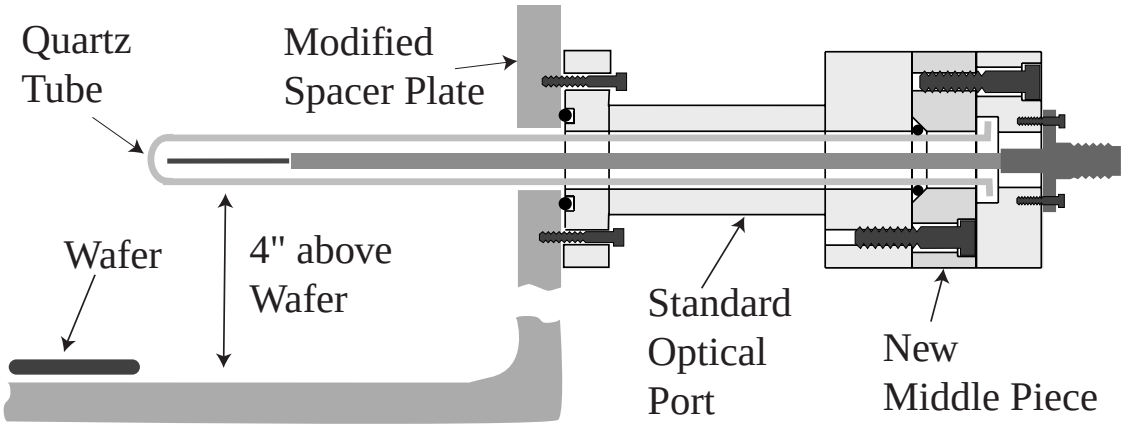

FIG. 2. Schematic of probe design for Lam 9400, exploiting existing modifications to spacer plate

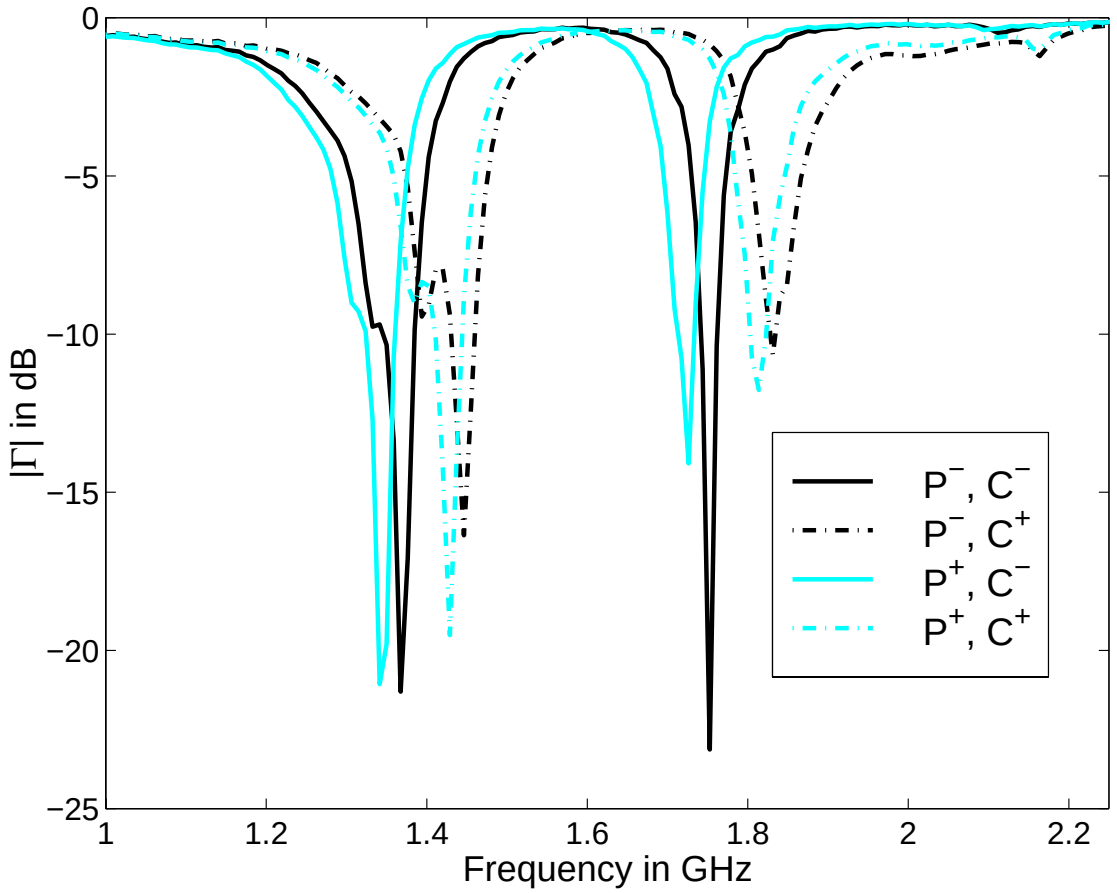

FIG. 3. Physical Vs. Chemical Etch Experiment: 'P': Physical Etch- '+', high bias and '-', low bias power, 'C': Chemical Etch - '+' etching chemistry, '-', passivating chemistry

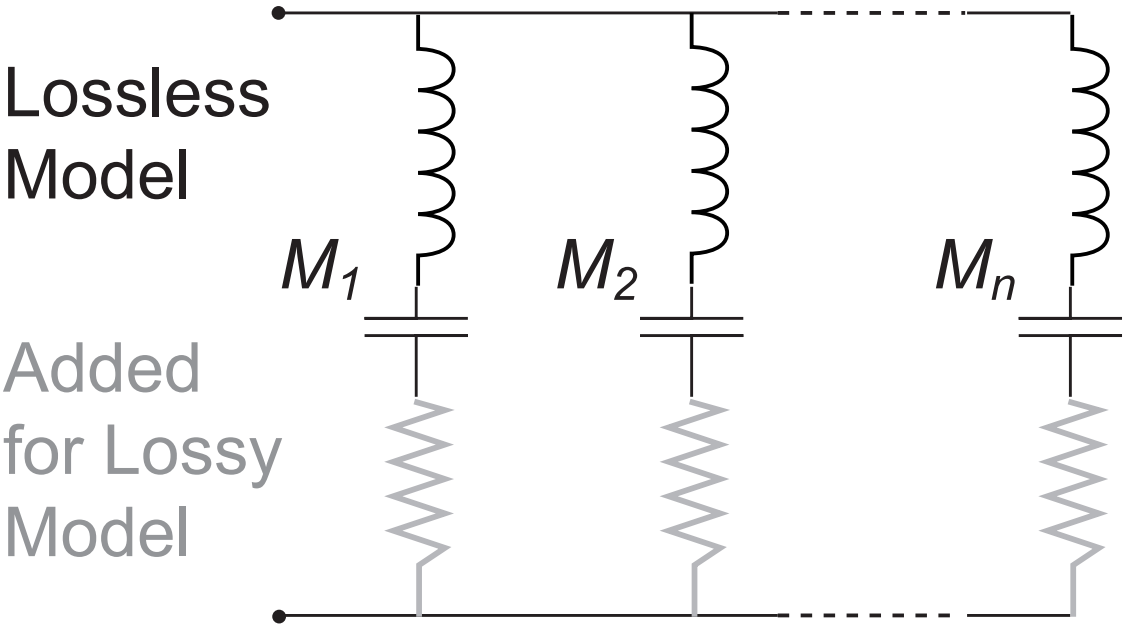

FIG. 4. Equivalent circuit model of multiple mode cavity resonator. LC circuits model lossless dielectric, added resistor models lossy dielectric.

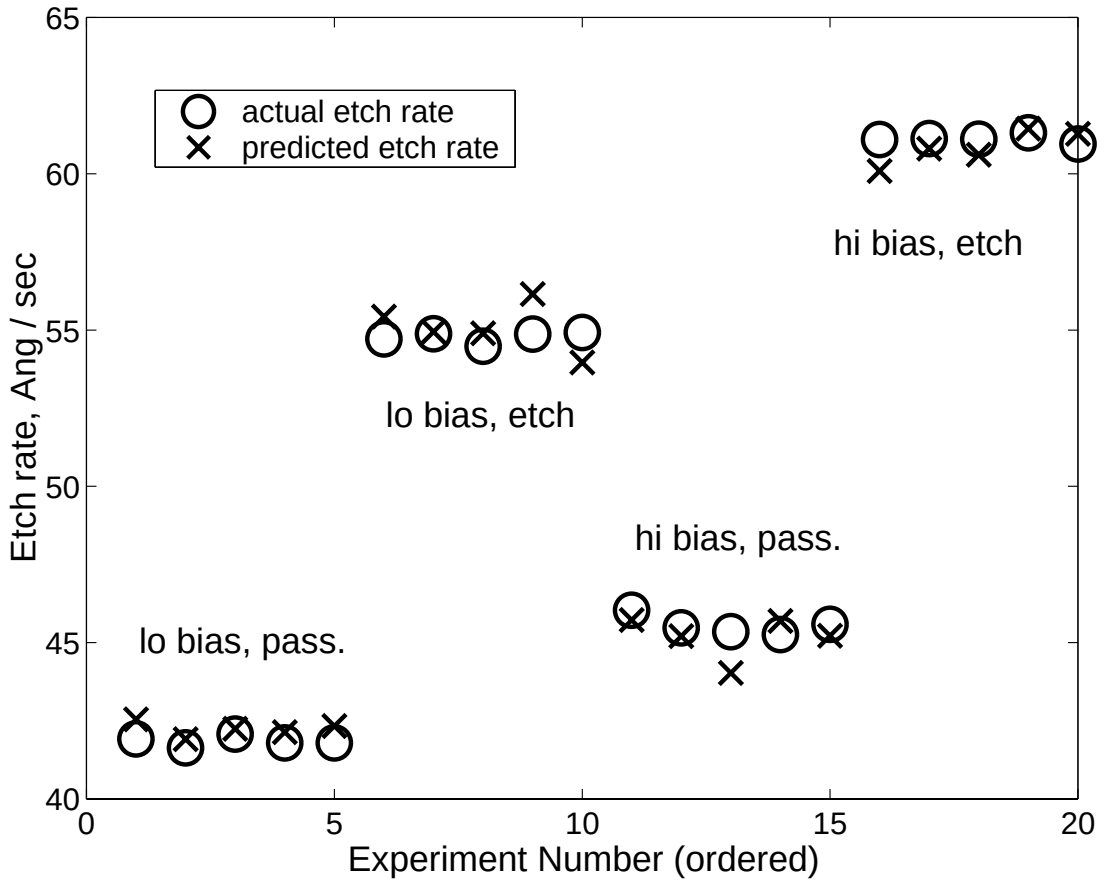

FIG. 5. Etch rate on blanket polysilicon wafers. Comparison of broadband model prediction and etch rate as measured by Leitz SP. Experiments are ordered by treatment combination, and experimental repetition.

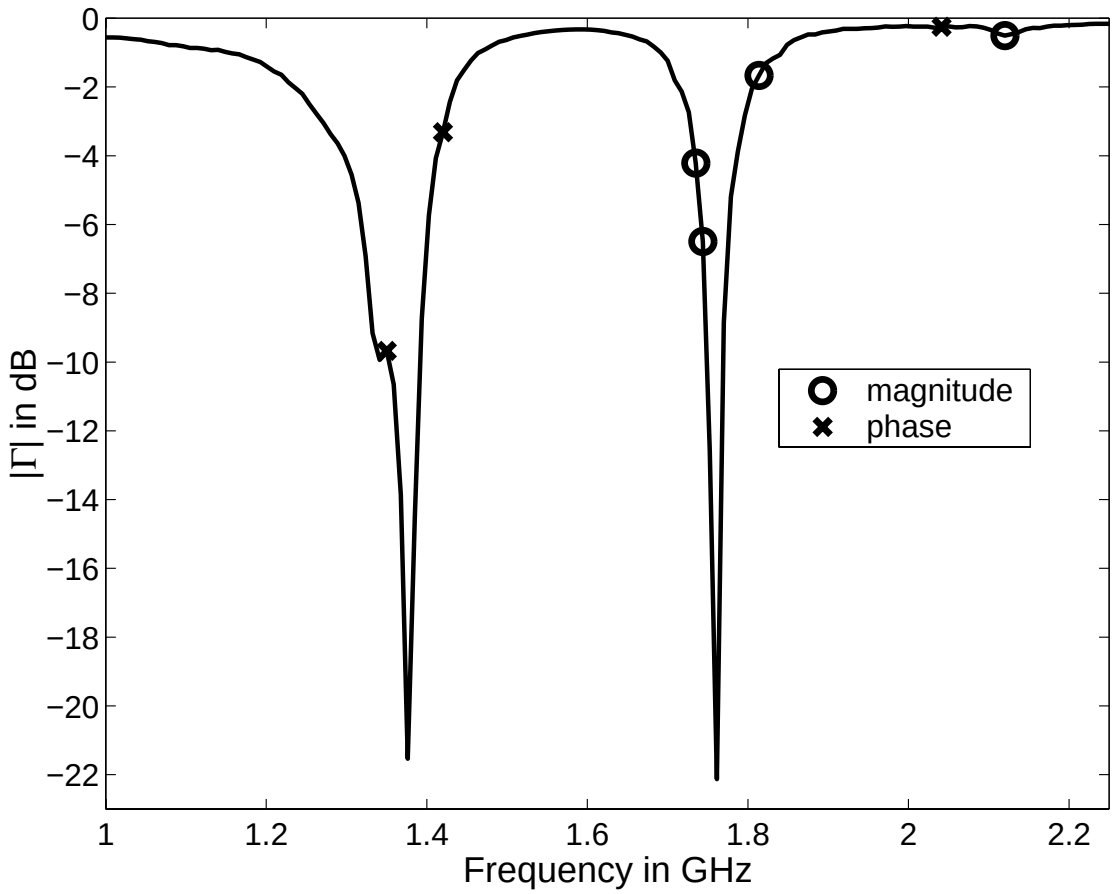

FIG. 6. Typical magnitude and phase points chosen for regression of etch rate from broadband response

TABLES

TABLE I. Process Input Levels Used for Second Etch DOE

Level	Press	Bias	TCP	Cl_2	HBr
1	10 mT	130 W	340 W	40 Sccm	100 Sccm
2	10 mT	190 W	340 W	100 Sccm	40 Sccm

TABLE II. Fit Resulting from Parameterized Response Model in Order of Contribution

model order	1	2	3	4	5
factor	$(\omega_n)_1^{'}$	R_1	Q_1	$\mathrm{VSWR}_1^{'}$	$(\omega_n)_2$
R^2	0.2382	0.597	0.814	0.911	0.962